

Journal of Photonics for Energy

SPIEDigitalLibrary.org/jpe

Enhancing light extraction in organic light-emitting devices via hemispherical microlens arrays fabricated by soft lithography

Sang-Hyun Eom
Edward Wrzesniewski
Jiangeng Xue

Enhancing light extraction in organic light-emitting devices via hemispherical microlens arrays fabricated by soft lithography

Sang-Hyun Eom, Edward Wrzesniewski, and Jianguo Xue

University of Florida, Department of Materials Science and Engineering, Gainesville,
Florida 32611-6400
jxue@mse.ufl.edu

Abstract. We demonstrate enhanced light extraction in organic light-emitting devices (OLEDs) by using microlens arrays fabricated by a soft lithography technique. A large-area and close-packed polystyrene (PS) monolayer was formed on the SiO₂ substrate using a convective-capillary assembly method, and a polydimethylsiloxane polymer was used to obtain a concave template, from which microlens arrays were fabricated from a photopolymerizable transparent optical adhesive. The microlens contact angle and array fill factor both depend on the size of PS microspheres, and nearly close-packed, hemispherical microlens arrays with microlens contact angle of $(85 \pm 5 \text{ deg})$ and array fill factor of $(85 \pm 3)\%$ were obtained with 100- μm PS microspheres. The enhancement in the light-extraction efficiency in OLEDs when such fabricated microlens arrays were attached to the light-emitting surface depends on the contact angle of microlens, device size, and detailed multilayer structure of the OLED. For a large-area ($12 \times 12 \text{ mm}$) fluorescent OLED with a near close-packed hemispherical microlens array, a maximum enhancement of $(70 \pm 7)\%$ in the light-extraction efficiency was achieved. © 2011 Society of Photo-Optical Instrumentation Engineers. [DOI: [10.1117/1.3528267](https://doi.org/10.1117/1.3528267)]

Keywords: organic light-emitting diodes; light-extraction efficiency; light-outcoupling efficiency; microlens arrays; soft lithography.

Paper 10151SSPR received Aug. 27, 2010; revised manuscript received Nov. 10, 2010; accepted for publication Nov. 15, 2010; published online Jan. 4, 2011.

1 Introduction

Since the first organic light-emitting devices (OLEDs) were introduced by Tang and Vanslyke,¹ tremendous research carried out by academia and industry over the past two decades has led to real commercial applications in displays and lighting.² The development of phosphorescent OLEDs (PHOLEDs), which can achieve nearly 100% internal quantum efficiency (η_{IQE}),³ made it possible to employ PHOLEDs for displays, typically operating at low brightness condition (luminance $L = 100 \text{ cd/m}^2$). However, PHOLEDs still have limitations in lighting applications, which require much higher efficiency (60–70 lm/W) and operating conditions ($L = 1000 \text{ cd/m}^2$) than those of displays.⁴ One of the major limiting factors is the low light-extraction efficiency of $\sim 20\%$ in planar structure PHOLEDs, due to the total internal reflection (TIR) losses at multiple interfaces.⁵

The significant amounts of photons that are trapped and lost in substrate, indium tin oxide (ITO)/organic, and localized plasmonic modes can be partially extracted using many different approaches,^{6–8} leading to enhanced light-extraction efficiency exceeding $\sim 20\%$. It is necessary to modify the internal structure of OLEDs in order to extract ITO/organic and localized plasmonic modes, whereas a simple texturing technique on the surface of the glass substrate or attaching a macrolens or a microlens array to the glass substrate^{9–14} can easily enhance the photon

extraction from substrate modes. For example, Sun and Forrest recently demonstrated highly ordered hemispherical microlens arrays using an imprint lithography method, showing high light-extraction enhancement of (1.68 ± 0.09) .⁷ However, complicated photolithography and wet-etching processes in making such a microlens mold is still considered to be an issue for the commercialization of microlens.

In this report, we introduce a rather simple microlens fabrication method with near perfect control on the microlens geometry and arrangement. A large-area and close-packed polystyrene (PS) monolayer was created using a convective and capillary assembly,¹⁵ and a soft lithographic molding technique was employed to generate a concave polydimethylsiloxane (PDMS) template for a reproducible polymer microlens. We found that high microlens contact angle of $(85 \pm 5 \text{ deg})$ and array fill factor (FF) of $(85 \pm 3)\%$ could be obtained using 100- μm PS microspheres. The application of such microlens arrays to the glass surface of the large-area OLED enhances the light-extraction efficiency up to $(70 \pm 7)\%$. We also show that the light-extraction efficiency of the OLED is affected by microlens contact angle, OLED size, and detailed layer structure of the OLED.

2 Experiment

The microlens fabrication procedures based on a soft lithography molding technique are illustrated in Fig. 1. PS microspheres in an aqueous solution (0.3% for 5 and 20 μm , 2.1% for 100 μm in solids content) were purchased from Thermo Fisher Scientific. All PS microspheres ($\phi_{\text{PS}} = 5, 20, \text{ and } 100 \mu\text{m}$) were monodispersed using a convective and capillary assembly on a precleaned hydrophilic UV-ozone-treated glass or SiO_2 substrate.¹⁵ The substrate was initially slightly tilted ($<10 \text{ deg}$) in order to create a downward convection flow when the aqueous solution with PS microspheres was continuously dropped, eventually leading to the PS monolayer (without convection flow, multilayered PS arrays are expected). When water evaporates from the PS monolayer side, strong capillary forces between PS microspheres can make tightly closed-packed PS arrays. In order to make a reproducible soft mold for a microlens array, the PDMS (Sylgard 184 purchased from Dow Corning) was mixed with 10:1 weight ratio (base polymer : curing agent) and poured onto the PS monolayer. The substrate was kept in vacuum for 3 h to completely remove the gas from the PDMS precursor and thermally cured for 2 h at 60°C in a vacuum oven. A highly transparent Norland optical adhesive [(NOA) 61, refractive index ~ 1.56 in cured polymer] is used for the polymer microlens material and directly dropped onto the concave surface of PDMS template a few times. The glass substrate of an OLED was then subsequently placed on top of NOA 61 and left for 2 min without any pressure to well

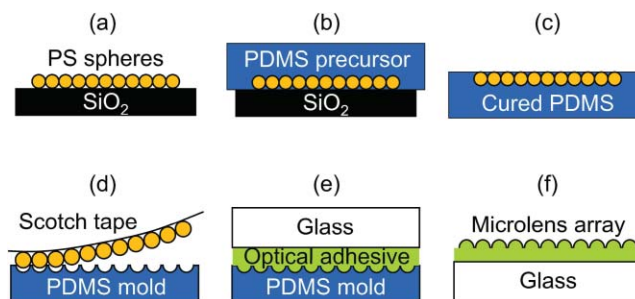


Fig. 1 Schematic illustration of the procedures for fabricating large-area and close-packed microlens arrays using a soft lithographic molding method. (a) Create a PS monolayer on Si substrate (coated with thin SiO_2 layer), (b) pour PDMS precursor onto the PS monolayer, (c) remove the substrate after thermal curing of PDMS, (d) remove the embedded PS spheres from the cured PDMS with scotch tape, (e) apply 2–3 drops of optical adhesive on the concave PDMS mold and place the glass side of the OLED on top of optical adhesive, and (f) release the PDMS mold after UV-curing of the optical adhesive, leaving behind microlens arrays. See text for details.

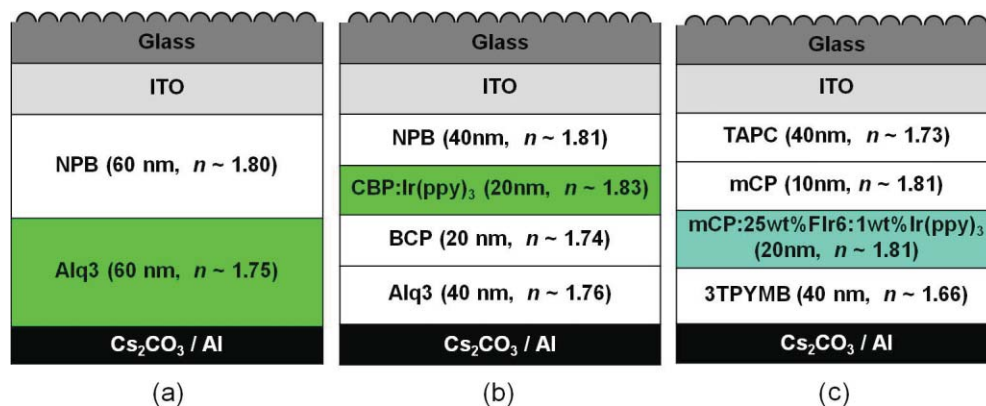


Fig. 2 Schematic device structures of (a) green FOLED, (b) green PHOLED, and (c) blue-green PHOLED. Refractive indices are measured by ellipsometry at their respective peak emission wavelengths (525 nm for the green FOLED, 510 nm for the green PHOLED, and 460 nm for the blue-green PHOLED).

spread out the NOA 61 before the UV-curing process ($\lambda = 365$ nm, 200 mW/cm² for 3 min). Separating the concave PDMS mold from the cured NOA 61 leaves behind the convex microlens arrays on the glass substrate of the OLED. The soft PDMS mold could be reused for many times without any breakage.

The light-extraction efficiency enhancement of OLEDs was examined by attaching the large-area (covering a circle ~ 2 -cm diam) microlens arrays to the glass surface of OLEDs, which have been fabricated using a vacuum thermal evaporation method following procedures published elsewhere.^{16,17} Also, two different sizes of OLEDs, 2×2 mm² (small area) and 12×12 mm² (large area), defined by the overlapping area of two electrodes in the cross-bar geometry, were fabricated. The multilayer device structures of fluorescent OLEDs (FOLEDs) and PHOLEDs are schematically illustrated in the Figs. 2(a)–2(c). The green FOLED structure consisted of glass/ITO/N, N'-bis(naphthalen-1-yl)-N,N'-bis(phenyl)-benzidine [(NPB), 60 nm]/tris(8-hydroxy-quinolinato)aluminum (Alq₃, 60 nm)/Cs₂CO₃ (1 nm)/Al (100 nm), and the green PHOLED structure was glass/ITO/NPB (40 nm)/8.0 wt.% *fac*-tris-(phenylpyridine) iridium [Ir(ppy)₃] doped 4,4'-N,N'-dicarbazole-biphenyl (CBP) (20 nm)/bathocuproine [(BCP), 20 nm]/Alq₃ (40 nm)/Cs₂CO₃ (1 nm)/Al (100 nm). A two-color (blue-green)-emitting PHOLED structure was also fabricated: glass/ITO/1,1-bis-(di-4-tolylaminophenyl)cyclohexane [(TAPC), 40 nm]/25 wt.% iridium(III) bis(4',6'-difluorophenylpyridinato)tetrakis(1-pyrazolyl) borate(Flr6) and 1.0 wt.% *fac*-tris-(phenylpyridine) iridium [Ir(ppy)₃]-doped N,N'-dicarbazolyl-3,5-benzene (mCP) (20 nm)/tris[3-(3-pyridyl)mesityl]borane [(3TPYMB), 40 nm]/Cs₂CO₃ (1 nm)/Al (100 nm).

Three different methods were applied to measure the outcoupling efficiency (η_{out}) enhancement between with and without microlens arrays. First, Si photodetector (818-UV, diameter = 1 cm) was used to measure the far-field luminous intensity at the normal direction assuming a Lambertian source, and calibrated using a luminance meter (Minolta LS-100 with No. 110 close-up lens). Current density (J) versus voltage (V) characteristics of the OLEDs were measured using an Agilent 4155C semiconductor parameter analyzer. Second, OLEDs were aligned and attached to the entrance port of a Newport integrating sphere (819D 3-Port), and an Ocean Optics Jaz spectrometer was connected to the outlet port to measure the total luminous flux from the OLEDs. Only the light-emitting device (LED) area was opened toward the inside of the integrating sphere, while all the other nonemitting areas were completely blocked. Third, an optical fiber sensor (Ocean Optics, diameter = 400 μ m) was used to measure the near-field luminous intensity at the normal direction, and the angular distribution of the luminous intensity was measured using a small-area Si spot photodetector (818-UV) at 10 cm away from the device (corresponding to a half angle of ~ 0.5 deg).

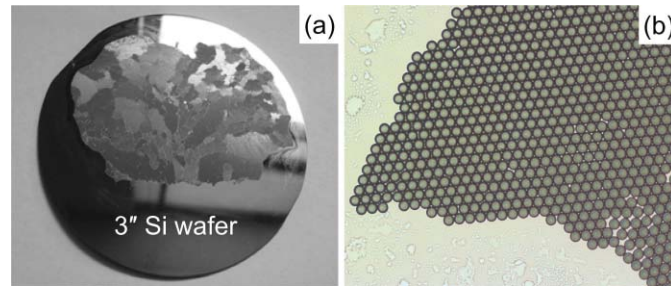


Fig. 3 (a) Convective and capillary assembly is employed to form a large-area PS microsphere monolayer on a 3-in. Si wafer (coated with a thin SiO_2 layer). (b) Optical microscope image of a PS microsphere monolayer. 100- μm -size PS microspheres are used in both (a) and (b).

3 Results and Discussion

3.1 Characterization of Microlens Arrays

A large-area PS microsphere monolayer on a 3-in. Si wafer fabricated by a convective and capillary assembly is shown in Fig. 3(a). Up to a few square inches of PS monolayer could be created. Although grain boundaries are observed between individually close-packed PS domains, hexagonally close-packed PS microsphere arrays are well formed as shown in Fig. 3(b). We observed that PS monolayers could be easily formed for 20- and 100- μm -size PS microspheres. However, it was more challenging to generate a large-area monolayer for 5- μm -size PS microspheres due to the increased impact of the capillary force; therefore, they are not used for the later device studies.

Figure 4(a) is a cross-sectional scanning electron microscopic (SEM) image showing the completely embedded PS microspheres in the cured PDMS after removing the substrate. The subsequent application of scotch tape could well remove the embedded PS microspheres and PDMS residues as shown in Fig. 4(b), leading to a concave PDMS mold successfully as shown in Fig. 4(c). A large-area microlens array using a PDMS mold is

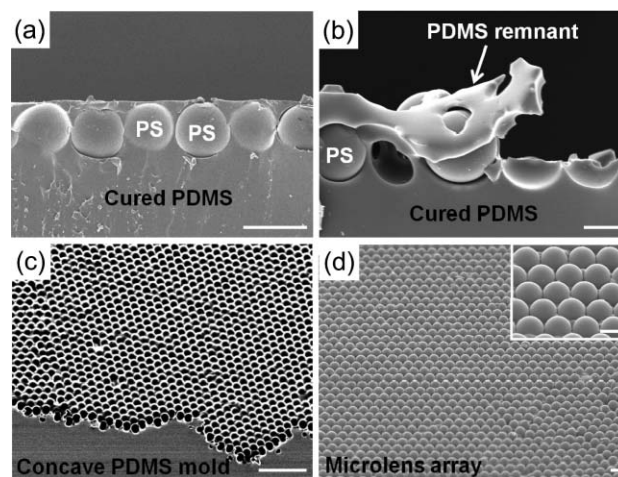


Fig. 4 (a) Cross-sectional SEM image of embedded 100- μm -size PS spheres in cured PDMS. (b) The PDMS mold after (intentional) incomplete removal of 20- μm -size PS spheres. (c) Concave PDMS template for microlens arrays after completely removing 20- μm -size PS spheres. (d) Large-area 100- μm -size microlens arrays subsequently made with the concave PDMS mold. Inset: hexagonally close-packed lens arrays are observed. Scale bar is 100 μm in (a), (c), and (d), and 20 μm in (b).

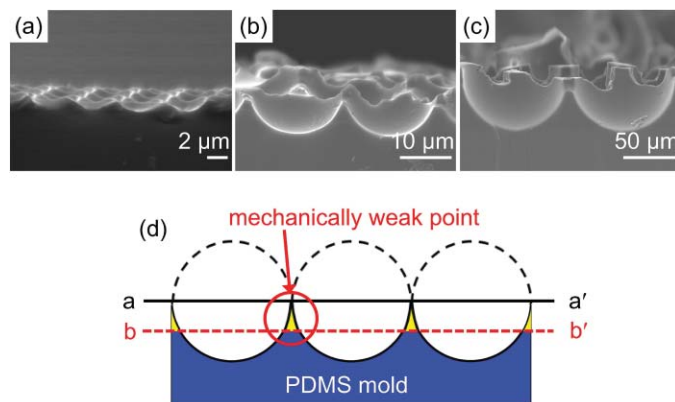


Fig. 5 Cross-sectional SEM images of concave PDMS molds fabricated using (a) $\phi_{PS} = 5 \mu\text{m}$, (b) $\phi_{PS} = 20 \mu\text{m}$, and (c) $\phi_{PS} = 100 \mu\text{m}$. (d) Schematic illustration of mechanically weak points in the PDMS mold when removing PS spheres from the cured PDMS. The PS separation is expected along the a-a' plane for 100- μm -size PS spheres, but along a lower plane (such as the b-b' plane) for smaller size PS spheres due to the (unwanted) removal of PDMS in the mechanically weak points.

shown in Fig. 4(d) and highly close-packed microlens arrays are also shown in the inset of Fig. 4(d). The measured FF of this microlens array (from 100- μm PS microspheres) is $(85 \pm 3)\%$, which is very close to the ideal FF of two-dimensional hexagonally close-packed spheres (91%).

The same microlens fabrication method could be applied to different sizes of PS microspheres; however, the contact angle θ_c of the PDMS mold is dependent on ϕ_{PS} as shown in the cross-sectional SEM images of Figs. 5(a)–5(c). As the size of PS microspheres was increased, the shape of PDMS mold was closer to the perfect hemisphere, showing almost hemispherical shape for $\phi_{PS} = 100 \mu\text{m}$. We believe that this is related to the mechanical robustness of the PDMS mold in the narrow regions between individual features. When the PDMS precursor was poured onto the PS microspheres in order to make a concave template, it could completely cover the PS microspheres, penetrating all the way down to the SiO_2 surface through the interstitials among the PS microspheres [see Fig. 4(a)], which after curing form columns connecting PDMS below and above the PS microspheres. When the scotch tape was applied to remove the PS microspheres from the thermally cured PDMS, it is ideal that PDMS breaks along the a-a' plane in Fig. 5(d), leaving concave hemisphere features in the mold. We believe that PDMS columns using $\phi_{PS} = 100 \mu\text{m}$ are mechanically robust and broken at the narrowest neck area along the a-a' plane. However, narrower columns using smaller ϕ_{PS} are more easily torn off at locations away from the narrowest neck area (for example, along the b-b' plane), resulting in height less than the PS microsphere radius and, in turn, lower contact angles for the PDMS mold.

The contact angles of microlens using different PDMS molds clearly showed the difference in θ_c as shown in Figs. 6(a)–6(c). Here, θ_c , averaged over more than 10 lenses, was obtained by drawing a tangential line at the edge of a lens and measuring its angle with the substrate surface. We obtained $\theta_c = (45 \pm 5 \text{ deg})$ with $\phi_{PS} = 5 \mu\text{m}$, which is similar to previous reports.^{18,19} As the ϕ_{PS} was increased to 20 and 100 μm , θ_c was increased to $(65 \pm 5 \text{ deg})$ and $(85 \pm 5 \text{ deg})$, respectively, as shown in Fig. 6(d). The semicircle drawn in the cross-sectional microlens image for $\phi_{PS} = 100 \mu\text{m}$ [see Fig. 6(c)] clearly shows the hemispherical shape of the lens. The FF of the microlens array was estimated by counting the number of lenses per unit area and measuring the base diameter of lens. The FF for the microlens array from $\phi_{PS} = 20 \mu\text{m}$ was only $(67 \pm 3)\%$, but increased to $(77 \pm 3)\%$ and $(85 \pm 3)\%$ for $\phi_{PS} = 20$ and 100 μm , respectively, as shown in Fig. 6(d).

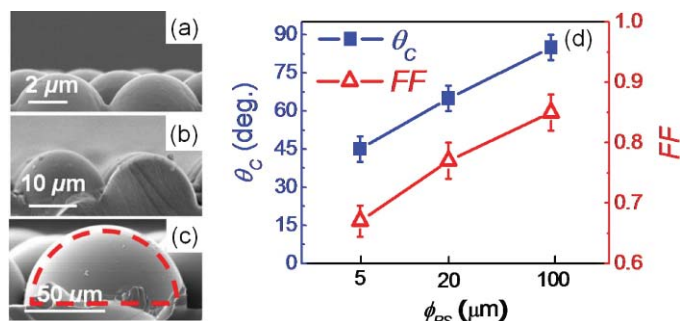


Fig. 6 Cross-sectional SEM images of convex microlenses with different sizes of PS spheres: (a) $\phi_{PS} = 5 \mu\text{m}$, (b) $\phi_{PS} = 20 \mu\text{m}$, and (c) $\phi_{PS} = 100 \mu\text{m}$. In (c), the dashed semicircle line is drawn for comparison. (d) The PS sphere size (ϕ_{PS}) dependence for the contact angle (θ_c) of microlens and the lens array fill factor (FF).

3.2 Enhancement in OLED Light Extraction due to Microlens Arrays

The light-extraction enhancement by microlens arrays (fabricated from 20- or 100- μm PS spheres) is investigated based on two different sizes of FOLEDs. For small-area ($2 \times 2 \text{ mm}^2$) FOLEDs, Fig. 7 shows the external quantum efficiencies (η_{EQE}) with and without microlens arrays based on 100- μm PS spheres. The η_{EQE} was obtained from the far-field luminous intensity measurement method and showed a light-extraction enhancement factor (defined as the light output with the microlens array to that without the microlens array) of $f = (1.35 \pm 0.04)$ in the entire current injection range. This enhancement factor, although confirming the applicability of using microlens arrays to enhance the light extraction in OLEDs, is somewhat lower than the previously reported enhancement factors using microlens arrays fabricated using other methods, which is in the range of 1.5–1.7 (Refs. 7 and 14).

Figure 8(a) compares the absolute luminous intensities for a large-area ($12 \times 12 \text{ mm}^2$) FOLED with or without a microlens array ($\phi_{PS} = 100 \mu\text{m}$). The FOLED is operated at $J = 5 \text{ mA/cm}^2$, in both cases, and measured using an integrating sphere system. By integrating the area under the peak in each spectrum, we obtained a light-extraction enhancement factor of $f = (1.70 \pm 0.07)$ with the microlens array, which was significantly higher than the result for the small-area FOLED. We believe such an OLED size dependence on f is attributed to the Al cathode size. When photons are reached at the air/microlens interface, some photons may be reflected back toward the cathode instead of escaping the front surface. A larger metal cathode can redirect those backward traveling photons again to the forward directions, enhancing

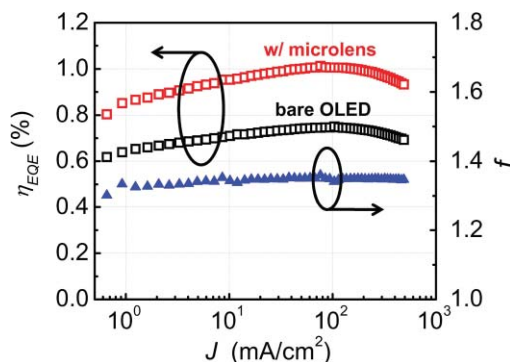


Fig. 7 External quantum efficiencies (η_{EQE}) of small-area FOLEDs with and without microlens arrays. Light-extraction enhancement factor (f) of (1.35 ± 0.04) is calculated as the ratio of the light intensity with the microlens array to that without the microlens array.

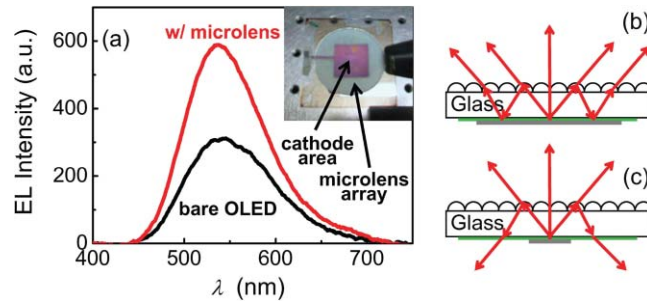


Fig. 8 (a) EL intensity difference with and without microlens arrays (fabricated from $\phi_{PS} = 100 \mu\text{m}$) for large-area FOLEDs ($12 \times 12 \text{ mm}$). EL intensities are measured with the device operated at 5 mA/cm^2 in both cases using an integrating sphere system. Inset: Photo of the large-area FOLED covered with a microlens array on the glass surface ($\phi_{PS} = 100 \mu\text{m}$). Schematic illustrations for light-extraction mechanism in (b) large-area and (c) small-area OLEDs with a microlens array attached to the glass substrate.

the chance of forward light extraction as illustrated in Fig. 8(b). However, with a smaller metal cathode as shown in Fig. 8(c), there is a significant backward air mode, leading to low light-extraction efficiency into the forward-viewing direction.

The enhancement factor for large-area devices was also confirmed by the near-field luminous intensity measurement. As shown in the inset of Fig. 9, only half of a large-area FOLED was covered with a microlens array ($\phi_{PS} = 100 \mu\text{m}$). With the device operated at $J = 3 \text{ mA/cm}^2$, the near-field optical intensity was recorded across the entire light-emitting area (between the bare side and the side covered with the microlens array) using an optical fiber that is perpendicular to the device. As illustrated in Fig. 9, we see that the electroluminescent (EL) intensity in the microlens covered region is ~ 1.69 times higher than that in the bare side of the OLED. This is in good agreement with the integrating sphere measurement results for large-area FOLEDs.

We have also studied the light-extraction enhancement in FOLEDs using microlens arrays fabricated from $20\text{-}\mu\text{m}$ PS microspheres. As summarized in Fig. 10, enhancement factors of $f = (1.25 \pm 0.04)$ and (1.45 ± 0.05) were obtained for small-area and large-area devices, respectively. In addition to the device area dependence as observed with larger microlenses, we also see that the absolute enhancement was somewhat lower in this case, as compared to using microlenses from $100\text{-}\mu\text{m}$ PS microspheres. We attribute this to the lower contact angles of microlenses from $20\text{-}\mu\text{m}$ PS microspheres rather than similar FF as shown in Fig. 6.

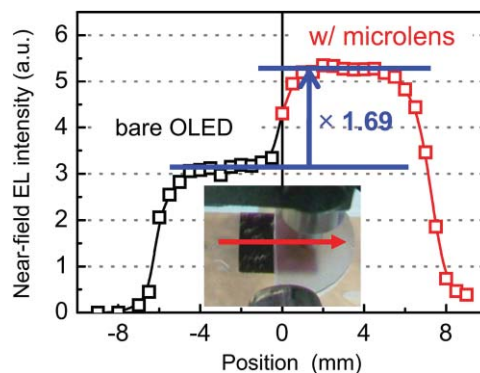


Fig. 9 Near-field luminous intensity profile across a large-area FOLED. The right half of the FOLED was covered with a microlens array, while the other half was bare. The FOLED was operated at 3 mA/cm^2 , and negligible degradation was confirmed before/after the measurement. The inset shows a picture of device in the measurement setup.

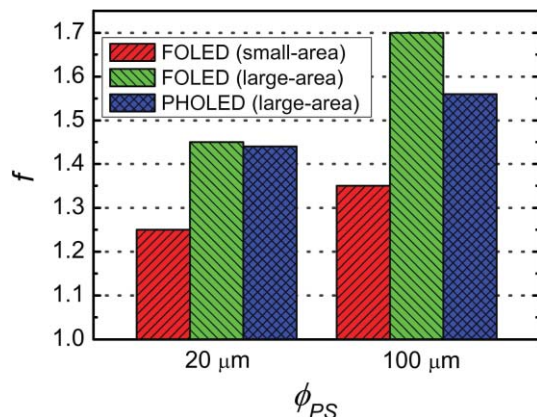


Fig. 10 Comparison of the light-extraction enhancement factor (f) for small-area (2×2 mm) and large-area (12×12 mm) FOLEDs and PHOLEDs, using microlens arrays fabricated from two different sizes of PS microspheres ($\phi_{PS} = 20$ and 100 μm).

Light-extraction efficiency can be enhanced significantly at larger angles than ~ 41.8 deg [critical angle for TIR at the air ($n = 1.0$)/glass ($n = 1.5$) interface with the planar glass] with the attachment of microlens arrays on the surface of glass substrate, and previous results showed that higher contact angle microlens can extract photons more effectively than by the lower contact angle microlens^{7,14}, which is consistent with our results here.

Figure 11 shows the angular emission patterns for the OLED with the microlens attachment ($\phi_{PS} = 100$ μm). High θ_c of microlens is obtained using standard procedure (see Section 2) with low-viscosity optical adhesive (NOA61, 300 cps), whereas low θ_c is intentionally fabricated by dropping high-viscosity optical adhesive (NOA 68, 5000 cps) onto the glass surface of the OLED and instant curing after putting down the PDMS mold. Although bare OLED showed a slightly wider angular emission pattern than a Lambertian source due to the measurement setup, slightly forward directional and a negligible pattern change were observed with high and low microlenses, respectively, compared to that of bare OLED. We believe tall height of high θ_c microlens arrays blocks the light emission at larger angles and redirects it forward, which is

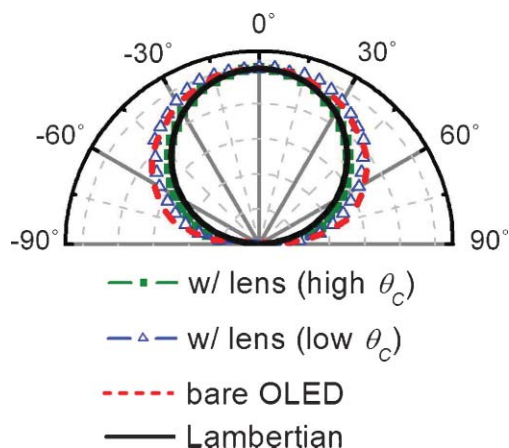


Fig. 11 Normalized optical power intensity as a function of the viewing angle for a bare FOLED (red dashed line) and FOLEDs with low and high contact angle microlens arrays (blue open triangles and green solid squares, respectively), as well as that for a Lambertian source (black solid line).

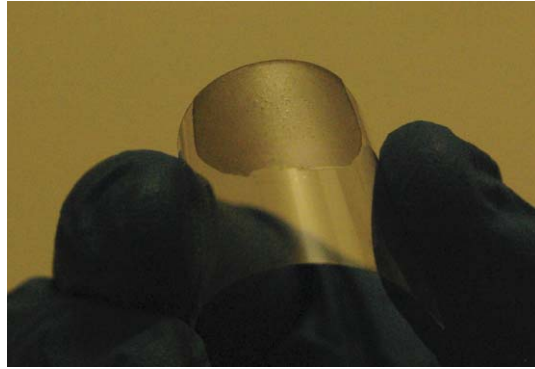


Fig. 12 Photograph of microlens arrays ($\phi_{PS} = 100 \mu\text{m}$) on a flexible PET substrate. The microlens fabrication method applied to the glass substrate could be also compatible with the flexible PET substrate.

opposite what Sun and Forrest demonstrated using $7\text{-}\mu\text{m}$ microlens arrays with the enhanced luminous intensities at larger angles (especially at $>40 \text{ deg}$).¹⁴

The close-packed hemispherical microlens arrays ($\phi_{PS} = 100 \mu\text{m}$) were also attached to the large-area PHOLEDs, and the light-extraction efficiency was examined using the near-field luminous intensity measurement method. Interestingly, somewhat lower $f = (1.56 \pm 0.06)$ was observed for both green and blue-green PHOLEDs compared to that for green FOLEDs ($f = 1.69 \pm 0.04$) as shown in Fig. 10. We attribute this difference to the more significant optical modes confinement for the PHOLEDs with higher refractive indices of the emissive layers ($n_{CBP} = 1.83$ at $\lambda_{\text{peak}} = 510 \text{ nm}$ and $n_{mCP} = 1.81$ at $\lambda_{\text{peak}} = 460 \text{ nm}$) than those of neighboring layers ($n_{NPB} = 1.81$ and $n_{BCP} = 1.74$, $n_{TAPC} = 1.73$ and $n_{3TPYMB} = 1.66$), measured by ellipsometry (see Fig. 2). Therefore, it is expected that less amount of photons could reach the glass substrate for the PHOLED, eventually leading to lower light-extraction enhancement by microlens arrays. The two PHOLEDs do exhibit nearly identical light-extraction enhancement factor, suggesting that the light-extraction mechanism we described here is not sensitive to the wavelength of emission; therefore, it could be potentially applied to white LEDs without altering the emission spectrum appreciably.

Note that the microlens arrays can be fabricated on the glass substrate prior to the deposition of the organic multilayer stack, which is on the other side of the glass substrate. Hence, it does not affect any possible degradation processes inside the OLED structure. The increased light-extraction efficiency does suggest that the OLED can be operated at a lower current and voltage in order to achieve the same operating brightness, which in turn prolongs the lifetime of the OLEDs.^{20,21} We have also tested the microlens array fabrication on the surface of the polyethylene terephthalate (PET) substrate for application to flexible OLEDs. Shown in Fig. 12 is a photograph of a PET substrate with a microlens array attached using the same procedure as described above for fabricating microlens arrays on glass substrates. Although we have not fabricated OLEDs on the PET substrate and, therefore, the light-extraction enhancement factor in flexible OLEDs due to the microlens array is unknown, this clearly shows that the microlens array fabrication process described here could be potentially integrated with roll-to-roll fabrication of OLEDs on flexible substrates.

4 Conclusions

We have shown that the light-extraction efficiency of FOLEDs can be improved up to 70% using large-area, close-packed hemispherical microlens arrays fabricated by a soft-lithography method. Different contact angles of the microlens are achieved with different sizes of PS microspheres, and contact angle of $(85 \pm 5 \text{ deg})$ and fill factor of $(85 \pm 3)\%$ are obtained using

100- μm PS microspheres. It is also found that a large cathode size is necessary to maximize the light extraction by microlens arrays due to the photon redirection into forward by the large-area aluminum cathode. For multilayered POLEDs, slightly low-light-extraction efficiency is observed with microlens arrays due to the significant optical modes confinement in the emissive layer. The microlens fabrication technique described here has a great advantage for application to large-area lighting systems, instead of pixelated small-area display devices.

Acknowledgments

The authors gratefully acknowledge financial support from the U.S. Department of Energy Solid State Lighting Program (Award No. 09EE0000990) and the Florida Energy Systems Consortium. S.H.E. also acknowledges a fellowship from Samsung SDI. Co., Ltd.

References

1. C. W. Tang and S. A. Vanslyke, "Organic electroluminescent diodes," *Appl. Phys. Lett.* **51**, 913–915 (1987).
2. S. R. Forrest, "The path to ubiquitous and low-cost organic electronic appliances on plastic," *Nature* **428**, 911–918 (2004).
3. C. Adachi, M. A. Baldo, M. E. Thompson, and S. R. Forrest, "Nearly 100% internal phosphorescence efficiency in an organic light-emitting device," *J. Appl. Phys.* **90**, 5048–5051 (2001).
4. S.-H. Eom, Y. Zheng, E. Wrzesniewski, J. Lee, N. Chopra, F. So, and J. Xue, "White phosphorescent organic light-emitting devices with dual triple-doped emissive layers," *Appl. Phys. Lett.* **94**, 153303 (2009).
5. H. Benisty, H. D. Neve, and C. Weisbuch, "Impact of planar microcavity effects on light extraction—Part 1: basic concepts and analytical trends," *IEEE J. Quantum Electron.* **34**, 1612–1631 (1998).
6. Y.-J. Lee, S.-H. Kim, J. Huh, G.-H. Kim, Y.-H. Lee, S.-H. Cho, Y.-C. Kim, and Y. R. Do, "A high-extraction-efficiency nanopatterned organic light-emitting diode," *Appl. Phys. Lett.* **82**, 3779–3781 (2003).
7. Y. Sun and S. R. Forrest, "Enhanced light out-coupling of organic light-emitting devices using embedded low-index grids," *Nat. Photon.* **2**, 483–487 (2008).
8. T. Shiga, H. Fujikawa, and Y. Taga, "Design of multiwavelength resonant cavities for white organic light-emitting diodes," *J. Appl. Phys.* **93**, 19–22 (2003).
9. E. Adachi, A. S. Dimitrov, and K. Nagayama, "Stripe patterns formed on a glass-surface during droplet evaporation," *Langmuir* **11**, 1057–1060 (1995).
10. S.-I. Chang and J.-B. Yoon, "Shape-controlled, high fill-factor microlens arrays fabricated by a 3D diffuser lithography and plastic replication method," *Opt. Express* **12**, 6366–6371 (2004).
11. C.-C. Cheng, C. A. Chang, and J. A. Yeh, "Variable focus dielectric liquid droplet lens," *Opt. Express* **14**, 4101–4106 (2006).
12. Y. Lu, Y. Yin, and Y. Xia, "A self-assembly approach to the fabrication of patterned, two-dimensional arrays of microlenses of organic polymers," *Adv. Mater.* **13**, 34–37 (2001).
13. S. Moller and S. R. Forrest, "Improved light out-coupling in organic light emitting diodes employing ordered microlens arrays," *J. Appl. Phys.* **91**, 3324–3327 (2002).
14. Y. Sun and S. R. Forrest, "Organic light emitting devices with enhanced outcoupling via microlenses fabricated by imprint lithography," *J. Appl. Phys.* **100**, 073106 (2006).
15. L. Malaquin, T. Kraus, H. Schmid, E. Delamarque, and H. Wolf, "Controlled particle placement through convective and capillary assembly," *Langmuir* **23**, 11513–11521 (2007).
16. S.-H. Eom, Y. Zheng, N. Chopra, J. Lee, F. So, and J. Xue, "Low voltage and very high efficiency deep-blue phosphorescent organic light-emitting devices," *Appl. Phys. Lett.* **93**, 133309 (2008).

17. S.-H. Eom, Y. Zheng, E. Wrzesniewski, J. Lee, N. Chopra, F. So, and J. Xue, "Effect of electron injection and transport materials on efficiency of deep-blue phosphorescent organic light-emitting devices," *Org. Electron.* **10**, 686–691 (2009).
18. H. J. Nam, D.-Y. Jung, G.-R. Yi, and H. Choi, "Close-packed hemispherical microlens array from two-dimensional ordered polymeric microspheres," *Langmuir* **22**, 7358–7363 (2006).
19. H. Yabu and M. Shimomura, "Simple fabrication of micro lens arrays," *Langmuir* **21**, 1709–1711 (2005).
20. J.-H. Lee, C.-I. Wu, S.-W. Liu, C.-A. Huang, and Y. Chang, "Mixed host organic light-emitting devices with low driving voltage and long lifetime," *Appl. Phys. Lett.* **86**, 103506 (2005).
21. D.-S. Leem, H.-D. Park, J.-W. Kang, J.-H. Lee, J. W. Kim, and J.-J. Kim, "Low driving voltage and high stability organic light-emitting diodes with rhenium oxide-doped hole transporting layer," *Appl. Phys. Lett.* **91**, 011113 (2007).

Sang-Hyun Eom received his B.S. (1999) from Hanyang University and M.S. (2001) from Pohang University of Science and Technology (POSTECH), South Korea, majoring in mechanical engineering. He worked at Samsung SDI from 2001 to 2006 as a display device design engineer and joined the University of Florida in 2006 to pursue his Ph.D. in materials science and engineering. His research at the University of Florida focuses on the development of high efficiency blue and white phosphorescent organic light-emitting devices (OLEDs) and enhancing the light extraction efficiency in OLEDs. Upon completion of his Ph.D. in December 2010, he is returning to the central research center in Samsung SDI, South Korea.

Edward Wrzesniewski is currently working towards his Ph.D. in Materials Science and Engineering at the University of Florida. He received his B.S. in Materials Science from Carnegie Mellon University in 2008. His current research work focuses on architecture modification and outcoupling enhancements to organic light emitting devices.

Jiangeng Xue received his Ph.D. in electrical engineering from Princeton University in 2005. He also received his B.S. (1995) and M.S. (1998) degrees in physics from University of Science and Technology of China (USTC). After working at Global Photonic Energy Corporation (Ewing, NJ) as a Research Scientist for nearly a year, he joined the University of Florida as an Assistant Professor in Materials Science and Engineering in 2005, and was promoted to Associate Professor in 2010. His research interests are broadly on the physics and processing of organic and hybrid organic-inorganic electronic materials and their applications in lighting, displays, photovoltaics, photodetection, and circuitry. He has over 40 journal publications and over 20 issued and pending patents.